Gold nanoparticle-doped TiO_2 semiconductor thin films : Gas sensing properties

Buso, Dario; Post, Michael; Cantalini, Carlo; Mulvaney, Paul; Martucci, Alessandro

Publisher's version / Version de l'éditeur:
https://doi.org/10.1002/adfm.200800864
Advanced Functional Materials, 18, 23, pp. 3843-3849, 2008

ADVANCED FUNCTIONAL MATERIALS

DOI: 10.1002/adfm.200800864

Gold Nanoparticle-Doped TiO_2 Semiconductor Thin Films: Gas Sensing Properties**

By *Dario Buso, Michael Post, Carlo Cantalini, Paul Mulvaney,* and *Alessandro Martucci**

TiO_2 sol–gel films doped with gold nanoparticles are used as both optical and conductometric sensors for the detection of CO and H_2. Tests performed at 360 °C show for the first time CO- and H_2-induced reversible variations in the optical absorption of thin TiO_2/Au sol–gel films. The absorbance changes are strongly dependent on both the testing wavelength and the film microstructure. Together with the sensing dynamics observed through an electric interface, it is possible to obtain a better understanding of the mechanisms involved in the detection of both gases. The presence of H_2 elicits almost ideal, step-like dynamic responses using conductometric detection.

1. Introduction

Nanostructured semiconductor metal oxides, such as SnO_2, ZnO, TiO_2, and NiO, are promising sensing materials for a wide range of gases and vapors. The enhanced sensing features are determined by the high chemical activity and porosity of the active materials, which are direct consequences of their nanostructure. Because of this, gas sensing capabilities depend critically on the synthesis method and parameters that allow for tailoring of selectivity and sensitivity toward the target species. These materials can be further developed into nanocomposites, which are materials where metal nanoparticles (NPs) are dispersed in a matrix of metal oxides. The NPs play both passive and active roles in the sensing process. The presence of NPs increases the active surface area and improves gas diffusion inside the film. Nanocomposites have physical properties that differ from those of the nanostructured single phase oxides and improve the conditions for sensing by reducing the electrical resistance and increasing the optical absorption. Metal NPs also show catalytic properties that can modify the analyte–oxide chemical interactions and enhance the sensing process.

In a previous paper we reported the synthesis of Au NPs with controlled morphology and homogenous dispersion inside a TiO_2 matrix obtained using the sol–gel method.[1] In the present work the samples have been tested as CO and H_2 detectors through an optical and a conductometric interface using different conditions of temperature and material microstructure. Comparison of the data obtained via this double interface permitted a better understanding of the mechanisms involved in the detection of such species using a TiO_2 sol–gel-based thin film.

2. Results

2.1. Morphological Characterization

A description of the microstructure, morphology, and optical properties of the TiO_2–Au nanocomposites used in this work has been published elsewhere.[1] The characterization reported here refers to those samples that have been tested as active layers for the optical and conductometric detection of CO and H_2, that is, TiO_2–Au films that underwent annealing up to 400 and 500 °C with Au NP content up to 8 wt%.

Figure 1 shows the absorption spectra of both films measured in the 300–800 nm region. Surface plasmon resonance (SPR) bands arising from the presence of Au spheres inside the films are evident in both cases, with a maximum amplitude at 604 and 620 nm for the samples annealed at 400 and 500 °C, respectively. The SPR wavelengths are red-shifted compared to those reported for Au spheres in water suspensions (in the 520–530 nm region) due to the high

[*] Prof. A. Martucci, Dr. D. Buso
Dipartimento di Ingegneria Meccanica Settore Materiali
Universita' di Padova
Via Marzolo 9
35131 Padova (Italy)
E-mail: alex.martucci@unipd.it
Dr. M. Post
Institute for Chemical Process and Environmental Technology
National Research Council of Canada
1200 Montreal Road, Ottawa, ON K1A 0R6 (Canada)
Prof. C. Cantalini
Dipartimento di Chimica e Materiali, Università dell'Aquila
I67040 Monteluco di Roio, L'Aquila (Italy)
Prof. P. Mulvaney
University of Melbourne, School of Chemistry
Parkville, VIC 3010 (Australia)

[**] Alessandro Martucci thanks the Universities of Melbourne and Padova for their support through the University academic exchange program, and Padova University through Progetto di Ateneo 2007.

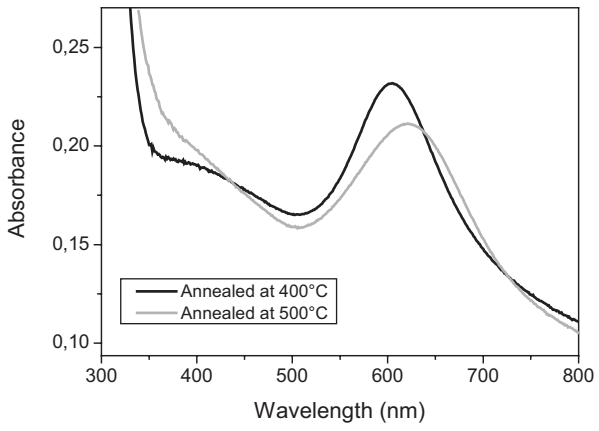

Figure 1. Optical absorption spectra of TiO_2 thin films containing Au NPs (8 wt%) after annealing at 400 and 500 °C.

refractive index of TiO_2 (in the range of 2.18–2.20 for these films).[1]

Figure 2 shows the surface morphology obtained from scanning electron microscopy (SEM) and atomic force microscopy (AFM) scans together with the X-ray diffraction (XRD) analysis performed in the $24° < 2\theta < 50°$ angular region with Cu-Kα radiation. XRD analysis shows the change in the TiO_2 matrix microstructure. While the TiO_2 matrix annealed at 400 °C is amorphous, after annealing at 500 °C the TiO_2 matrix assumes the anatase crystalline structure, as evident from the presence of the (101) and (200) anatase diffraction peaks.[2] XRD analysis also shows the presence of crystalline Au, evident from the diffraction signals arising from the (111) and (200) Au lattice planes.[3] Comparing the AFM and SEM images it can be seen that in the film heated to 500 °C there are larger crystalline domains composed of smaller crystalline nanograins with an average diameter of about 10 nm, in agreement with the crystallite anatase size estimated from the XRD line broadening.[1] The SEM image also revealed a residual porosity in the film, which is in agreement with the ellipsometry data reported in the previous paper.[1]

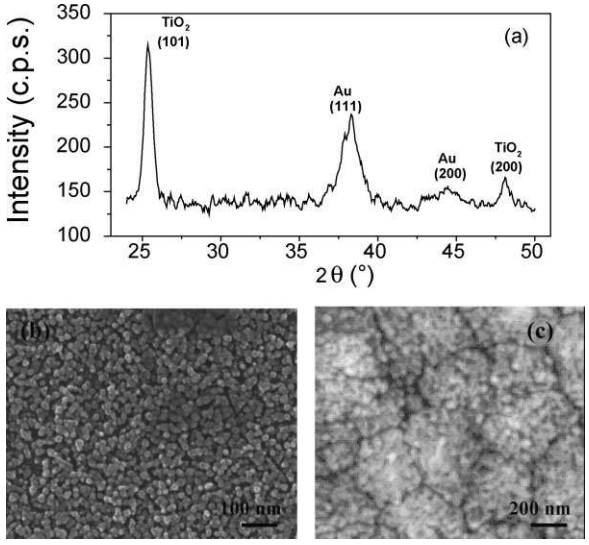

Figure 2. a) XRD patterns of TiO_2–Au films annealed at 500 °C. Diffraction peaks from Au (111) and (200) lattice planes and anatase (101) and (200) lattice planes are detectable. Crystalline grain dimensions evaluated with the Scherrer correlation yield a crystalline diameter of 5 nm for Au NPs and 11 nm for anatase. b) SEM image and c) AFM image of TiO_2-Au film annealed at 500 °C.

2.2. Optical Gas Sensing

The effect of high temperature exposure to 1% v/v CO and 1% v/v H_2 in air upon the optical absorbance of the films has been studied using a custom built gas flow chamber directly coupled inside a commercial spectrophotometer. Absorption spectra of films measured in air alone have been compared to those acquired while flowing the target gases inside the measuring chamber, and the resulting plots are shown in Figure 3 for a testing temperature of 360 °C. Figure 3a and b refer to samples annealed at 400 and 500 °C, respectively. Reversible gas-induced variations in the film absorption spectra were observed for both CO and H_2 exposure. The spectral changes to the absorption spectra involved primarily the SPR band, however the changes observed varied for each gas. In the case of samples annealed at 400 °C (Fig. 3a), exposure to CO did not induce appreciable shifts in the SPR band position, while the surface plasmon band blue-shifted in the presence of H_2 compared to the peak position observed in air. A similar gas-induced shift of the SPR peak was also observed for Au–TiO_2 films annealed at 500 °C (Fig. 3b) with a more pronounced response toward CO compared to that observed with the samples annealed at 400 °C. Undoped TiO_2 films annealed at 400 and 500 °C showed no optical absorption changes upon exposure to the target gases.

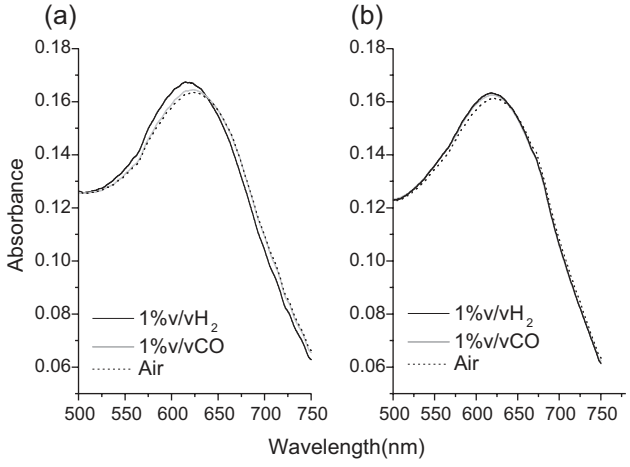

Figure 3. Optical absorbance spectra of films annealed at 400 °C (a) and 500 °C (b) measured in air (dotted line) and during exposure to 1% v/v CO (gray line) and 1% v/v H_2 (black line) at 360 °C operative temperature. The figure highlights the effect of gas exposure on the SPR frequencies of Au NPs (500–750 nm region).

The effects of the gases are more clearly seen in differential absorbance spectra, where we plot the gas-induced optical change ratio (OCR). The OCR is defined as the difference between the absorbance measured in air (A_{air}) and during gas exposure (A_{gas}), normalized to the absorbance level in air ($OCR = [A_{air} - A_{gas}]/A_{air}$). Figure 4 reports the OCR values for films annealed at 400 °C (Fig. 4a) and 500 °C (Fig. 4b) that have been exposed to 1% v/v CO and 1% v/v H_2. Films annealed at 400 °C are almost insensitive to CO exposure, while after annealing at 500 °C the response to both H_2 and CO is comparable, although less intense. Figure 5 reports dynamic responses of the TiO_2–Au films following exposure to 1% v/v of each gas measured at 590 and 730 nm. The temporal response to 1% v/v H_2 is more pronounced, while the signal in the presence of the same amount of CO is lower in both plots. At both wavelengths the film responds to CO with a square output signal, while the H_2 gas-to-air transient is affected by a slower recovery of the baseline. The initial air-to-gas transient is fast under exposure to both gases ($\tau_{90,CO} = 10$ s, $\tau_{90,H2} = 9.6$ s, defined as the time required to reach 90% of saturation signal after gas exposure), while the baseline recovery in the gas-to-air transient remains fast in the case of CO (15 s) but is very slow for H_2 (up to 8 min). Plots in Figure 5c and d show the same test performed on samples annealed at 500 °C. In this case the response dynamics for CO are different. The sensitivity is increased while the gas-to-air transient shows the same temporal evolution already observed in the case of H_2 exposure. This can be related to a triggering of a different detection mechanism, which in turn slows the baseline recovery dynamics due to slow desorption of the reaction products formed at the active detection sites.[4]

2.3. Conductometric Gas Sensing

The electrical resistance of TiO_2–Au films annealed at 400 and 500 °C upon exposure to increasing CO concentration is reported in Figure 6. Samples have been tested at an operative temperature of 300 °C in all cases, and dynamic responses have been obtained at gas concentrations in the 5–300 ppm range in dry air. Both samples showed a reversible and reproducible decrease of electrical resistance when exposed to the target gas at all concentrations, the film annealed at 500 °C giving a more stable signal with a lower noise level. Considering the reducing nature of CO, the electrical resistance decrease observed upon gas exposure is consistent with n-type semiconducting behavior of the TiO_2–Au nanocomposites. Au undoped TiO_2 films annealed at 400 and 500 °C were also tested but no appreciable variations in resistance were detected upon exposure to the target gases.

Figure 7 reports the dynamic response obtained upon exposure of the two films to increasing H_2 concentrations at 300 °C (8.5–510 ppm range in dry air). The signal shape is remarkably square, and reaction by-product desorption dynamics do not affect the gas-to-air transient. This fast and reproducible signal baseline recovery is ideal for gas sensing. Furthermore, the high stability of the resistance levels both in air and upon gas exposure allow for a quantitative resistance-

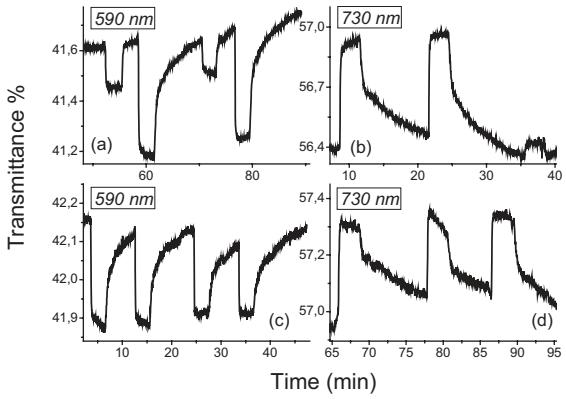

Figure 5. Dynamic response of TiO_2–Au films annealed at 400 °C (a) and (b) and 500 °C (c) and (d) at fixed wavelengths (590 and 730 nm) under exposure to air-gas-air cycles. Gas concentration was kept at 1% v/v for both CO and H_2.

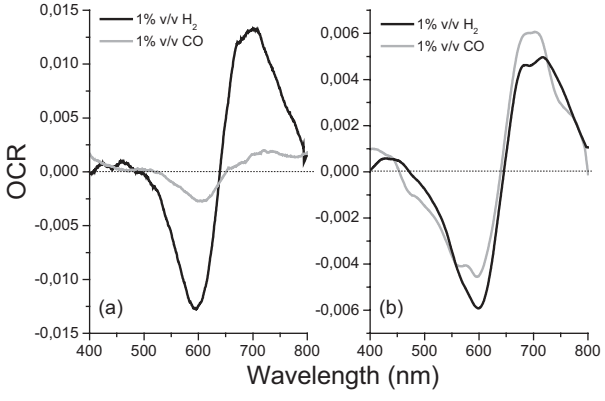

Figure 4. $OCR = [A_{air} - A_{gas}]/A_{air}$ of films annealed at 400 °C (a) and 500 °C (b) after exposure to 1% v/v CO and 1% v/v H_2 at 360 °C operative temperature.

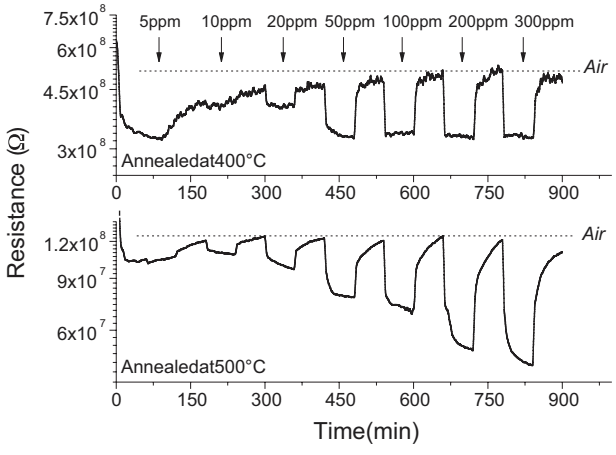

Figure 6. Dynamic response of films annealed up to 400 and 500 °C under CO exposure at increasing concentration levels in the 5–300 ppm range. Data measured at 300 °C.

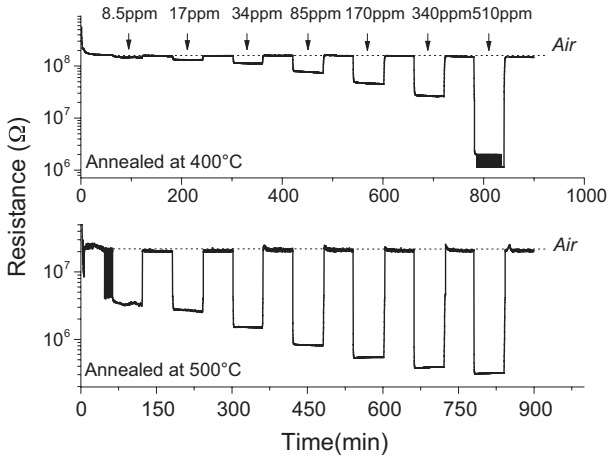

Figure 7. Dynamic response of films annealed at 400 and 500 °C under H_2 exposure at increasing concentration levels in the 8.5–510 ppm range. Data measured at 300 °C.

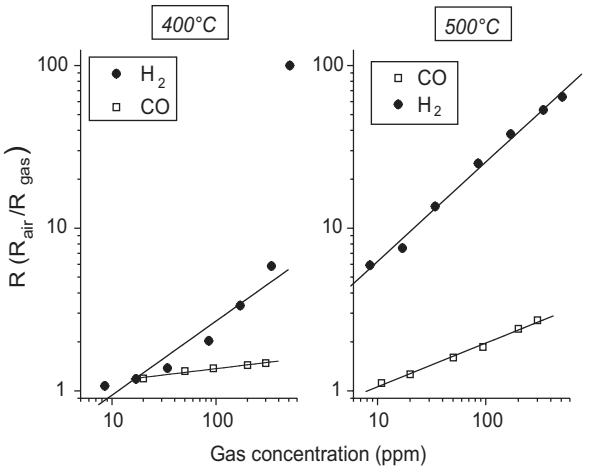

Figure 8. Response and relative sensitivity comparison between the film annealed at 400 °C (left) and at 500 °C (right) in detection of H_2 and CO. Operative temperature is 300 °C. Scale of plots is logarithmic.

to-gas concentration calibration. The response rates (τ_{90}) measured in both the air-to-gas and gas-to-air transients are remarkably fast, and are reported in Table 1. These are average values evaluated at the various gases concentrations and are characterized by a 6% maximum dispersion around the average time value.

The calibration curves relative to the sensing performance of the two sets of samples are reported in Figure 8 in terms of relative response ($R = R_{air}/R_{gas}$) versus gas concentration. The plots provide further evidence of the higher sensitivity of the films toward detection of H_2, as well as the higher sensing performance of those annealed at 500 °C. In this case, the resistance in the presence of H_2 is one order of magnitude lower than the values in air.

The influence of relative humidity (RH) on the film resistance in dry air was evaluated in the 150–300 °C temperature range on films annealed at 500 °C, and results are reported in Figure 9. At each testing temperature the films undergo exposure to dry air–humid air (RH 50%)–dry air cycles lasting 3 h each. The semiconductive behavior of the samples is demonstrated by the decreasing resistance levels in air at increasing temperatures. Humid air induces an increase in the conductivity of the films under all testing conditions, and behaves as a de facto reducing agent, as explained later in further detail. Figure 10 shows a similar test conducted at

Table 1. Response rates measured during dynamic exposure of TiO_2–Au films annealed at 400 and 500 °C to sequential air–gas–air cycles. The data refer to the air-to-gas ($\tau_{90,ads}$) and gas-to-air ($\tau_{90,des}$) time transients averaged over the total number of exposure cycles.

	CO detection		H_2 detection	
	$\tau_{90,ads}$ [min]	$\tau_{90,des}$ [min]	$\tau_{90,ads}$ [min]	$\tau_{90,des}$ [min]
Film annealed at 400 °C	3.8	7.5	0.4	2
Film annealed at 500 °C	11.6	39	0.06	1.3

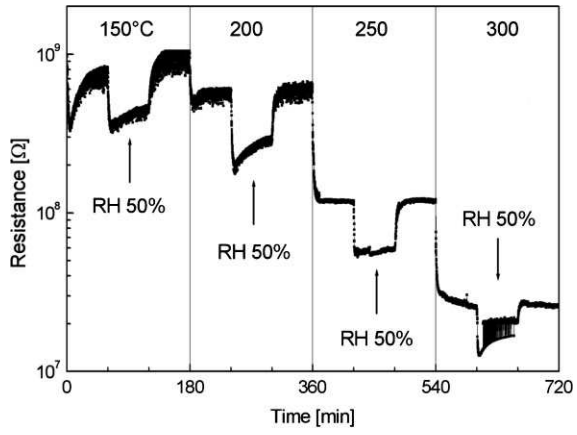

Figure 9. Resistance change induced by wet air (50% RH) with film annealed at 500 °C at operative temperatures in the range of 150–300 °C.

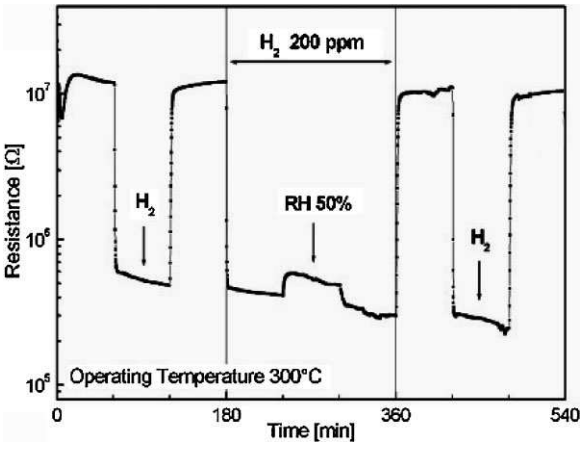

Figure 10. Effect of RH during detection of H_2 at 300 °C. Left and right side show response to H_2 in dry air as a reference. The mid-section shows interference of wet air (50% RH) during detection of 200 ppm of H_2. Measurement at 300 °C.

ADVANCED FUNCTIONAL MATERIALS

300 °C, in which the effect of 50% RH has been evaluated while detecting 200 ppm H_2. The test performed is a three step procedure: steps 1 and 3 consist of a cycle dry air–H_2–dry air performed in order to control the stability of the baseline signal before and after introducing the humidity perturbation, while step 2 is a gas in dry air–gas in humid air–gas in dry air cycle aimed at evaluating the effect of a humidity variation during gas detection. During the test a 50% humidity air mixture was fluxed inside the testing chamber while detecting 200 ppm H_2 in dry air. An increase in the film resistance was immediately observed with respect to the saturation signal obtained in dry air. This effect is in apparent contradiction with the data recorded in the absence of the target gas.

3. Discussion

The data presented constitute the first measurements of optical detection of CO and H_2 using a thin film TiO_2 sensor. Figure 3 and 4 demonstrate that a blue-shift in the SPR frequencies of Au NPs is provoked upon exposure to CO and H_2. This can be explained in terms of the transfer of electrons from the gases to the Au nanocrystals embedded within the titania catalyst. The donated electrons cause a decrease in the Au metal bulk plasma wavelength λ_p through

$$\lambda_{peak}^2 = \lambda_p^2(\varepsilon_\infty + 2\varepsilon_m) \quad (1)$$

where ε_∞ is the high-frequency dielectric constant of Au, ε_m is the dielectric constant of the medium, and λ_p is defined as[5]

$$\lambda_p = \sqrt{\frac{4\pi^2 c^2 m \varepsilon_0}{Ne^2}} \quad (2)$$

In Equation 2, N is the electron concentration, m the effective mass of conduction electrons, ε_0 is the vacuum permittivity, e is the electron charge, and c is the velocity of light. Changes in the particle electron density (N) can alter the plasmon frequency causing a shift in the band position. However, this does not allow us to unambiguously clarify the reaction mechanism. The reactant gases CO and H_2 may initially adsorb to the titania matrix. Once oxidized the liberated electrons then flow to and are trapped on the gold nanocrystals. Moreover, according to Equation 2, gas adsorption in the matrix sites near the NPs could lead to local changes in refractive index of TiO_2, which, in principle, are capable of affecting the spectral changes.

In the case of CO oxidation it has been proposed that Au might be directly involved in the kinetics of detection through selective adsorption of the target gas.[6–8] Multiple Au sites have been recognized to be capable, for example, of CO adsorption: some positively charged or vacant sites in the Au lattice, as well as the other peripheral sites adjacent to the oxide support, are considered to be preferential sites for CO adsorption and for the formation of carbonate species.[9] Moreover, adsorption studies performed using oxygen isotopes revealed that oxygen itself plays an active role in the overall process. In particular, oxygen coming from the oxide support has been shown to be involved in the formation of the carbonate-like species on the Au surface, while the oxygen atoms incorporated in the molecular carbon dioxide (oxidation product) come mainly from the gas phase. Therefore, two independent pathways are possible: i) oxygen reacts directly with CO at the surface of the Au NPs after activation in the form of a superoxo, O_2^-, or peroxo, O_2^{2-}, species, leading to the formation of molecular CO_2; and ii) oxygen from the support lattice at the NP–oxide boundaries interfaces, activates, or enhances the reactivity of adsorbed CO species.[7,10]

In the case of H_2 sensing, chemisorption processes may induce charge transfer between Au NPs and the supporting matrix.[7] It has been shown, for example, that H_2 can adsorb on n-type oxide semiconductors (such as TiO_2 and ZnO) in the form of a fully ionized electron donor and increase the population of the V_0^+ levels, which were previously depleted as a result of the presence of the metal particles.[11] This in turns appears to give a suitable explanation of the H_2-induced SPR band shift without invoking oxidative processes involving the gas molecules. Unlike CO, the available literature on H_2 catalytic oxidation on TiO_2–Au systems (leading to water production) is very limited. Additionally, a series of papers describe the preferential oxidation of CO over H_2 when catalyzed by TiO_2–Au systems.[12–17] Despite this, a number of authors report studies on the nature of adsorbed species over the TiO_2–Au systems during reaction of H_2 and O_2.[18,19] It was demonstrated that on nanosized Au clusters, hydrogen and oxygen react to form one or more hydrogen peroxide and surface hydroperoxy species.[8,18–21] At operative temperatures in the 250–300 °C range they found evidence for formation of H_2O_2 and of a hydroperoxo radical on the Au NP surface, where the latter is likely to form a hydrogen bonded complex with water or bind directly to the oxide surface. They also registered the presence of water molecules on the Au surface, which is consistent with the fact that H_2O_2 readily decomposes to water unless an acid or surface protons are present to stabilize it.[18] Thus, they concluded that the observed hydroperoxo radical must be either bound to Au or complexed with water resulting from decomposition of H_2O_2.

Figure 4 provides further evidence for the different behavior of the two films toward detection of the two gases. As observed before, the initiation of CO detection for the film annealed at 500 °C is related to the microstructural evolution of the TiO_2 matrix, which is amorphous after annealing at 400 °C but shows the anatase crystalline structure after annealing at 500 °C. This difference is important, as it permits further postulates about the different detection mechanism toward the two gases. In the case of CO, it is known from the literature that anatase–Au systems are capable of promoting CO oxidation at operative conditions similar to those adopted here,[22] and therefore it is plausible to conclude that the sensitivity enhancement toward CO detection depends on CO catalytic oxidation at the anatase–Au interface.[10,23,24] Furthermore, it is plausible that

formation of anatase triggers the catalytic oxidation of CO to CO_2, while in the case of H_2 the detection via catalytic oxidation is also promoted when TiO_2 is amorphous.

Gas sensing measurements performed using a conductometric interface offer further information to better highlight the detection mechanism of the two species. As observed before, the resistance drop observed under gas exposure is consistent with the n-type semiconductor behavior of films considering that CO and H_2 are reducing agents. This clearly shows that more charge carriers are available for electronic conduction and that there is sufficient mobility inside the nanocomposite to produce a detectable change in the resistivity. Since the electrical resistance of a material is not directly related to its refractive index, this observation is consistent with an increase of N in Equation 2 that produces a blue-shift of the Au NP plasmon frequencies.

The signal dynamics for CO detection, as reported in Figure 6, are characterized by a fast response rate when the gas is introduced into the testing chamber and by an acceptable recovery of the baseline after gas evacuation. The film annealed at 400 °C shows a much more squared response compared to that presented by the film annealed at 500 °C, which displays a more delayed gas-to-air transient. It is therefore acceptable to consider that diffusional issues or slow desorption of reaction by-products (in case of catalytic oxidation of CO to CO_2 triggered by formation of anatase) may arise when the porosity of the TiO_2 matrix drops to 30%, as measured for this film via ellipsometry/optical absorption.[1] A substantial difference between the two dynamics reported in Figure 6 can be observed by comparing the resistance levels at the various gas concentrations. While the film annealed at 500 °C shows a continuous increase of the gas-induced resistance change at increasing gas concentrations, the resistance drops measured using the film annealed at 400 °C appear to be of the same order of magnitude even though the CO concentration is increasing, especially at $[CO] \geq 50$ ppm. This could be interpreted as an effect due to the non-stability of the signal baseline measured in air, which is evidently not horizontal, or it could be related to a saturation of the adsorption sites for CO inside the sensing material.[4] The same trend observed in the case of optical CO detection is here replicated: while the film annealed at 400 °C does not show definite and reliable gas sensing properties toward CO detection, the one annealed at 500 °C shows a substantially better response. In this case the triggering of the catalytic oxidation of CO induced by formation of anatase around the Au NPs could also be postulated.

The dynamic response during H_2 exposure shows a remarkable ability of TiO_2 thin layers containing Au NPs to provide H_2 conductometric sensing materials. The sensing dynamics shown here exclude any diffusional limitation of H_2 inside the sol–gel layer, and in terms of the overall detection mechanism the reaction step is therefore dominant in the overall kinetic process. As reported in Table 1, the dynamic performance in both the air-to-gas and the gas-to-air transients are fast, presenting values on the order of seconds. It is shown here that the sol–gel technique is a useful and reliable synthetic strategy for the production of active materials for gas sensors. In this specific case, moreover, the designed sensor architecture of a porous matrix supporting active NPs yields highly effective sensor films that present a performance equal to that available commercially in terms of sensing dynamics.[25]

Data listed in Table 1 allow some observations about diffusional issues involved in the detection of both species to be made due to differences in the film morphology and microstructure. In general, the air-to-gas transient is faster than that observed for gas-to-air at all gas concentrations and for both of the two films tested. As found before,[4] this is kinetically explained by the presence in the desorption transient of the slower flux of the reaction by-products or adsorbed species from the active reaction sites. Moreover, as expected, it is evident that transient rates measured in the case of H_2 detection are higher than those characterizing the sensing dynamics of CO. An explanation for this is that the H_2 molecule is much smaller than CO, thus resulting in higher diffusional mobility inside the TiO_2 matrix. Diffusion limitations are evident in the case of CO as both transients are slower in the film annealed at 500 °C compared to those measured for the sample annealed at 400 °C. This is not the case for H_2 sensing with the film annealed at 500 °C, where faster dynamics in both transients are demonstrated in comparison with the film annealed at 400 °C.

The CO and H_2 gas sensitivity, represented by the slope of the linear response of Figure 8, improves after annealing at 500 °C. The film annealed at 500 °C shows better CO sensitivity with respect to the film annealed at 400 °C due to the formation of anatase as previously discussed. H_2 sensitivity of the film annealed at 500 °C is remarkably higher compared to CO gas sensitivity. At 100 ppm, H_2 and CO sensitivity yield $S = 28$ and $S = 2$, respectively.

Cross-sensitivity tests to evaluate the influence of RH% during H_2 sensing have been performed in dry air and while detecting H_2. The change of film resistance in dry and wet air (50% RH) and at an operating temperature in the range of 150–300 °C is reported in Figure 9. The resistance in dry air, hereafter referred to as the baseline resistance of the sensors (dotted lines), decreases with increasing operating temperature from 150 to 300 °C. A decrease in electrical resistance as a result of higher RH is registered at all temperatures. It is well known that at room temperature (25 °C) the conduction mechanism of films in the presence of water is ionic, where water molecules chemisorb on the material surface in the form of hydroxyl groups.[26] The first layer of physisorbed water is then doubly hydrogen bonded to the chemisorbed hydroxyls. The conduction mechanism is due to the hopping of protons between the physisorbed water molecules according to the Grotthuss proton chain reaction mechanisms.[27] However, at around 250 °C the response mechanism to humidity is electronic. At this temperature physisorbed water has been removed and water behaves like a reducing gas. The result of the interaction between water molecules and the sensor surface is that electrons are donated to the material and the electrical

response is determined by the intrinsic semiconducting properties of the material.[28] Because both water molecules and H_2 act as reducing gases, there seems to be an apparent contradiction given the smaller overall resistance decrease (step 2 of Fig. 10) compared to the H_2 resistance decrease (step 1 of Fig. 10). However, if we account for the smaller sensor sensitivity to water with respect to H_2 (compare the step at 300 °C of Fig. 9 with step 1 of Fig. 10) it turns out that the overall resistance decrease in step 2 of Figure 10 is controlled by water adsorption, which eventually inhibits H_2 response.

4. Conclusions

TiO_2 sol–gel films doped with Au NPs exhibited both optical and conductometric gas sensing capabilities, which were reversible and reproducible. Conductometric gas sensors showed very good response to H_2 with an almost ideal kinetic response for the absorption and desorption steps. For CO detection the formation of anatase in the TiO_2 films annealed at 500 °C is necessary to initiate the catalytic oxidation of CO and enhance the gas sensing response.

5. Experimental

The synthesis of the gold colloidal solution and the TiO_2 sol–gel films has been reported elsewhere [1]. Previously reported TEM measurement showed a mean diameter of 9.7 nm for the Au NPs with a standard deviation of 0.9 nm [1]. Films were deposited by spinning on a silica glass slide or on Si/Si_3N_4 substrates with Pt interdigital electrodes. Samples underwent annealing just after the deposition and were heated in air for 30 min at 400 or 500 °C. Typical thickness of the films, evaluated by ellipsometry measurements, were between 40 and 50 nm.

Extinction spectra of films deposited on silica glass slides were collected using a Cary 5 UV–vis–NIR spectrometer in the 200–800 nm wavelength range. Films were characterized by XRD using a Philips diffractometer equipped with glancing-incidence X-ray optics. The analysis was performed using Cu-Kα Ni filtered radiation at 40 kV and 40 mA. AFM and SEM were used to characterize the film surface.

The optical response of films induced by reducing gas species is monitored by means of a custom built heater mounted in a controlled gas flow chamber. The design of the apparatus permits unimpeded radiation transmission through the whole assembly. A Varian Cary1E spectrophotometer is used to detect transmission data in the 400–800 nm wavelength range with the films heated at selected values from 25 to 350 °C. Gas flow is automatically controlled in order to get continuous CO or H_2 flow inside the measurement chamber at concentrations up to 1 vol% in dry air. The substrate size for these measurements was approximately 10 mm × 20 mm and the incident spectrophotometer beam was normal to the film surface and covered a 6 mm × 1.5 mm area.

The electrical response of films to H_2 and CO gases was measured by an automated system. Dry air was mixed by an MKS147 multigas mass controller (MKS Instruments Inc.) with diluted H_2 mixture (1000 ppm in air) and CO mixture (1000 ppm in air) in order to have gas concentrations at the outlet in the range of 10–1000 ppm in dry air carrier gas. Different RH concentrations in the range of 0–80% were obtained by mixing dry air with saturated air at 25 °C and controlling the RH downstream by a MultiRAE gas monitor system (RAE Systems) with an accuracy of ±3% RH. Electrical measurements were carried out at the operating temperature of the films in the temperature range of 25–350 °C and at different gas concentrations. The resistance of the films was measured using a Keithley 2001 multimeter and a two-wire technique.

Received: June 26, 2008
Revised: September 16, 2008
Published online: November 18, 2008

[1] D. Buso, J. Pacifico, A. Martucci, P. Mulvaney, *Adv. Funct. Mater.* **2007**, *17*, 347.
[2] *Powder diffraction File*, International Center for Diffraction Data, Newton Square, PA, no. 86–1157.
[3] *Powder diffraction File*, International Center for Diffraction Data, Newton Square, PA, no. 04–0784.
[4] I. Lundström, *Sens. Actuators B* **1996**, *35*, 11.
[5] P. Mulvaney, L. M. Liz-Marzán, M. Giersig, T. Ung, *J. Mater. Chem.* **2000**, *10*, 1259.
[6] F. Boccuzzi, A. Chiorino, *J. Phys. Chem.* **1996**, *100*, 3617.
[7] F. Boccuzzi, A. Chiorino, S. Tsubota, M. Haruta, *J. Phys. Chem.* **1996**, *100*, 3625.
[8] H. Dyrbeck, N. Hammer, M. Ronning, E. A. Blekkan, *Top. Catal.* **2007**, *45*, 21.
[9] M. Haruta, S. Tsubota, T. Kobayashi, H. Kageyama, M. J. Genet, B. Delmon, *J. Catal.* **1993**, *144*, 175.
[10] M. Haruta, M. Dat, *Appl. Catal. A* **2001**, *222*, 427.
[11] J. L. Gersten, L. Wagner, A. Rosenthal, Y. Goldstein, M. Many, R. E. Kirby, *Phys. Rev. B: Condens. Matter* **1984**, *29*, 2458.
[12] J. Steyn, G. Pattrick, M. S. Scurrell, D. Hildebrandt, M. C. Raphulu, E. van der Lingen, *Catal. Today* **2007**, *122*, 254.
[13] J. Rasko, J. Kiss, *Catal. Lett.* **2006**, *111*, 87.
[14] D. L. Trimm, *Appl. Catal. A* **2005**, *296*, 1.
[15] C. Rossignol, S. Arrii, F. Morin, L. Piccolo, V. Caps, J. L. Rousset, *J. Catal.* **2005**, *230*, 476.
[16] W. Y. Yu, C. P. Yang, J. N. Lin, C. N. Kuo, B. Z. Wan, *Chem. Commun.* **2005**, *3*, 354.
[17] M. M. Schubert, V. Plzak, J. Garche, R. J. Behm, *Catal. Lett.* **2001**, *76*, 143.
[18] C. Sivadinarayana, T. V. Choudhary, L. L. Daemen, J. Eckert, D. W. Goodman, *J. Am. Chem. Soc.* **2004**, *126*, 38.
[19] M. Okumura, Y. Kitagawa, K. Yamagcuhi, T. Akita, S. Tsubota, M. Haruta, *Chem. Lett.* **2003**, *32*, 822.
[20] A. J. Bielanski Haber, *Oxygen in Catalysis*, Marcel Dekker Inc., New York **1991**.
[21] D. P. Dissanayake, J. H. Lunsford, *J. Catal.* **2002**, *206*, 173.
[22] J. M. C. Soares, P. Morrall, A. Crossley, P. Harris, M. Bowker, *J. Catal.* **2003**, *209*, 17.
[23] M. Haruta, *Gold Bull.* **2004**, *37*, 27.
[24] M. Haruta, *Catal. Today* **1997**, *36*, 153.
[25] See, for example, Commercial H_2 Gas Sensors, www.kebaili.com/pdkhs100.cfm (accessed October 2008) or H_2 Sensors Developed by NASA www.brc.nasa.gov/WWW/chemsensors/Gas%20Sensors%201201.htm (accessed October 2008).
[26] C. Cantalini, M. Pelino, *J. Am. Ceram. Soc.* **1992**, *75*, 546.
[27] H. Anderson, G. A. Parks, *J. Phys. Chem.* **1968**, *72*, 3662.
[28] C. Cantalini, M. Faccio, G. Ferri, M. Pelino, *Sens. Actuators B* **1994**, *19*, 437.